

Microstructural study of equiatomic PtTi martensite and the discovery of a new long-period structure

G.-M. Rotaru^a, W. Tirry^a, P. Sittner^b, J. Van Humbeeck^c, D. Schryvers^{a,*}

^a EMAT, University of Antwerp, CGB, Groenenborgerlaan 171, B-2020 Antwerpen, Belgium

^b Institute of Physics, Academy of Sciences, Prague 18221, Czech Republic

^c MTM, K.U.Leuven, Kasteelpark Arenberg 44, B-3001 Heverlee (Leuven), Belgium

Received 12 February 2007; received in revised form 5 April 2007; accepted 5 April 2007

Available online 1 June 2007

Abstract

The martensitic phase in an equiatomic PtTi alloy was studied by electron microscopy, neutron and X-ray diffraction, and differential scanning calorimetry. The expected orthorhombic B19 structure with Type I twinning on {111} planes was found plus a new $3\bar{3}$ long-period microtwin stacking based on this B19 structure, also including plate twinning. The measured microtwin volume fraction for the B19 is found to be larger than the value calculated from crystallographic theory, which can be explained by the fact that no martensite lattice parameters at the transformation temperature are known. An atomic model is suggested for the new long period structure in agreement with the electron diffraction and high resolution electron microscopy data.

© 2007 Acta Materialia Inc. Published by Elsevier Ltd. All rights reserved.

Keywords: PtTi; Shape memory alloys; Transmission electron microscopy (TEM); Twinning; Martensitic phase transformation

1. Introduction

Shape memory alloys are a special class of materials in which the martensitic phase transformation plays a crucial role. Most alloys with practical applications (such as NiTi and Cu-based alloys) exhibit a first-order transformation between -100 and 100 °C. In several potential practical applications, such as combustion engines or the control of high-temperature chemical reactions, however, there is a need for transformations at much higher temperatures. One of the potential alloys transforming at these elevated temperatures was reported by Donkersloot and Van Vucht [1] to be PtTi. This system exhibits, at and around the equiatomic composition, a martensitic transformation around 1000 °C from the cubic CsCl-type (B2) structure to the orthorhombic AuCd-type (B19) structure. The lattice correspondence between the austenite phase and the martensite phase and the related transformation behaviour were

described by Otsuka and Ren [2] as a shear shuffle of the $(110)_{B2}$ basal plane along the $[1-10]_{B2}$ direction, as shown in Fig. 1.

The martensitic phase transformation in this alloy occurs in a broad range of composition from 46 to 55 at.% Pt with a maximum M_s at 50 at.% Pt. The crystal structure transformation mechanism is similar to that in PdTi and NiTi, which have attracted much interest from theoreticians as well as experimentalists. Because of these similarities, the PtTi system has also become attractive for theoretical studies, and predictions of the atomic coordinates as well as reports of the martensitic structure [3,4] have been in good agreement with results obtained from earlier experiments based on X-ray diffraction [1,5]. The remaining experimental data are mostly dedicated to mechanical properties and the transformation temperature dependence vs. composition [6–9]. All these experimental results recommend this alloy as a promising high-temperature shape memory alloy possibly with the addition of ternary elements to improve the oxidation resistance and change the transformation temperatures. A proper characterization and understanding

* Corresponding author. Tel.: +32 3 2653247; fax: +32 3 2653257.

E-mail address: nick.schryvers@ua.ac.be (D. Schryvers).

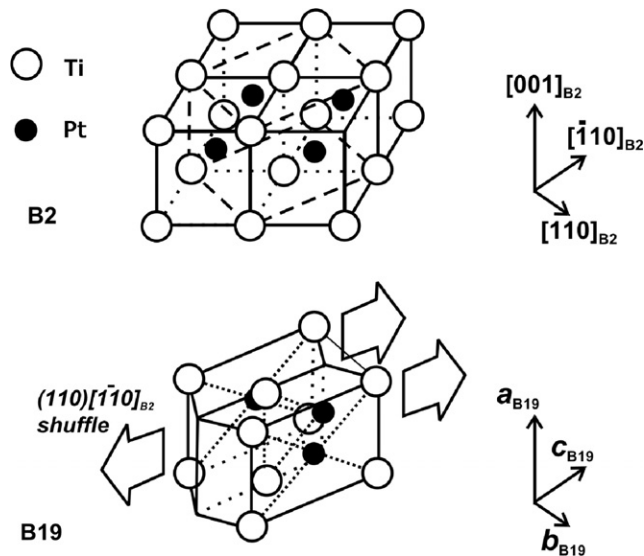


Fig. 1. The parent crystal structure at high temperatures (B2) and the lattice correspondence with the product (orthorhombic B19 structure) at lower temperature (after Otsuka and Ren [2]).

of the atomic structure and microstructure would further encourage potential applications based on this alloy.

The purpose of the present paper is to report on the atomic structure and microstructure of the basic B19 martensite structure and of a new $3\bar{3}$ long-period microtwin phase. Results are based on conventional transmission electron microscopy (TEM), selected area electron diffraction (SAED) and high-resolution TEM (HRTEM) plus some selective energy dispersive X-ray (EDX) analysis, supported by X-ray and neutron powder diffraction and differential scanning calorimetry (DSC).

2. Experimental procedures

The alloy was prepared by arc melting of the individual elements (99.99%) under a protective argon atmosphere. Mass loss measurements indicate an alloy with an average Ti content between 49.55 and 50.11 at.%. TEM samples were obtained by spark cutting 3 mm diameter discs ground to a thickness of approximately 150 μm , followed by homogenization in an evacuated quartz tube at 1250 $^{\circ}\text{C}$ for 1 h and water quenching to room temperature [10]. Thinning to electron transparency was done by ion-milling in some cases followed by light etching in an aqua regia solution to remove ion radiation damage [10]. Due to this omnipresent radiation damage, not many well-thinned areas could be found.

DSC measurements were performed in a NETZSCH DSC 404 instrument at MTM-K.U.Leuven. TEM and EDX were performed on a Philips CM20-twin microscope equipped with an Oxford atmospheric thin window INCAx-sight detector, while HRTEM observations were obtained using a JEOL 4000EX electron microscope equipped with a top-entry stage and operating at 400 kV, all at the EMAT Laboratory of the University of Antwerp.

The simulated electron diffraction patterns and HRTEM images were obtained using the MacTempas program for electron microscopy simulations based on the multislice method including dynamical interactions.

The X-ray powder diffraction was performed on a Philips X'Pert diffractometer equipped with a high-temperature chamber. Neutron powder diffraction was performed at a texture diffractometer at the nuclear reactor source at NPI Rez Prague on a cube sample of $2 \times 2 \times 2 \text{ mm}^3$ cut from the as-cast material.

3. Results

A DSC heating–cooling cycle starting at room temperature reveals two clear endothermic peaks upon heating, one small, with an onset at 1016 $^{\circ}\text{C}$ and an area of -2.7 J g^{-1} , and one larger, with an onset at 1035 $^{\circ}\text{C}$ and an area of -23.4 J g^{-1} , as shown in Fig. 2. The cooling branch reveals a single large exothermic peak, with an onset at 1015 $^{\circ}\text{C}$ and an area of 28.7 J g^{-1} , and a very shallow exothermic bump around 987 $^{\circ}\text{C}$. The larger peaks upon heating and cooling can be expected to correspond with the known B2 to B19 martensitic transformation with a hysteresis of 20 $^{\circ}\text{C}$ [1]. Moreover, when returning in the cycle from between the two endothermic peaks in the heating curve, the large exothermic peak no longer appears but the shallow bump remains. Likewise, when stopping the cooling cycle just above the shallow exothermic bump and returning to higher temperatures, the small endothermic peak at 1016 $^{\circ}\text{C}$ no longer appears. The latter two experiments indicate that the small endothermic peak and the shallow exothermic bump belong to the same reversible transformation.

TEM confirms that the alloy at room temperature is completely in the martensite state with a grain size around 100 μm and without any indication of precipitation of a third phase. The experimental diffraction patterns reveal two types of structures. The first corresponds with the

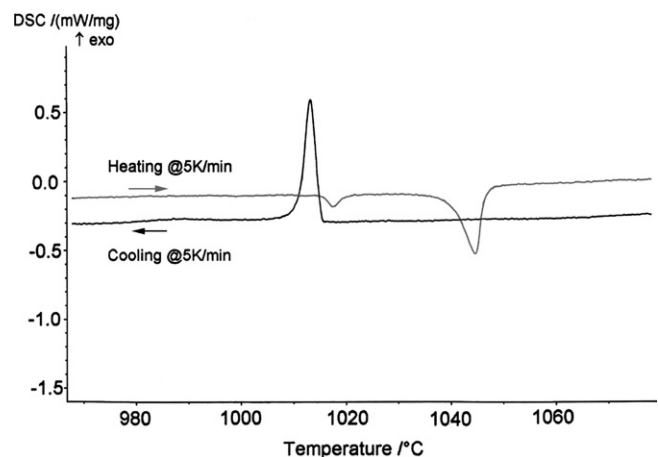


Fig. 2. Heating and cooling traces of the DSC run revealing a small and a large endothermic peak and a large exothermic peak plus a shallow exothermic bump.

reported B19 structure [1,3–5], with lattice parameters, as measured from the present SAED patterns, of $a_{B19} = 0.275 \pm 0.005$ nm, $b_{B19} = 0.456 \pm 0.008$ nm, $c_{B19} = 0.49 \pm 0.02$ nm, and appears in multiply twinned plates with Type I macrotwinning on $(1\bar{1}1)$ planes, as seen from the dark field image and corresponding SAED pattern in Fig. 3. The second one has multiple reflections and weak streaks characteristic for a quasi-periodic long-period microtwinning along one of the basic axes (Fig. 4). The latter figure also

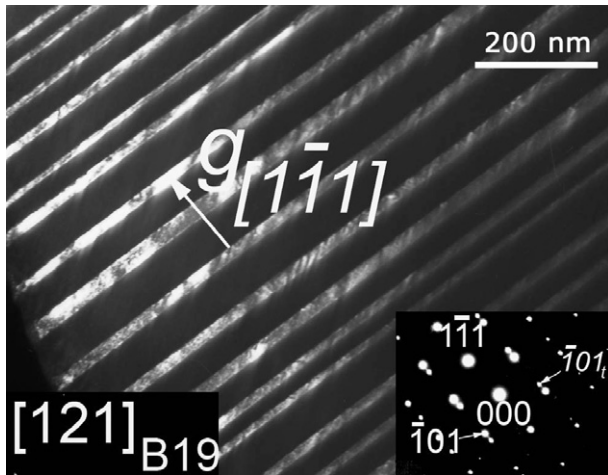


Fig. 3. Typical DF image revealing the $\{111\}$ twins in the B19 orthorhombic structure and the corresponding SAED pattern as inset.

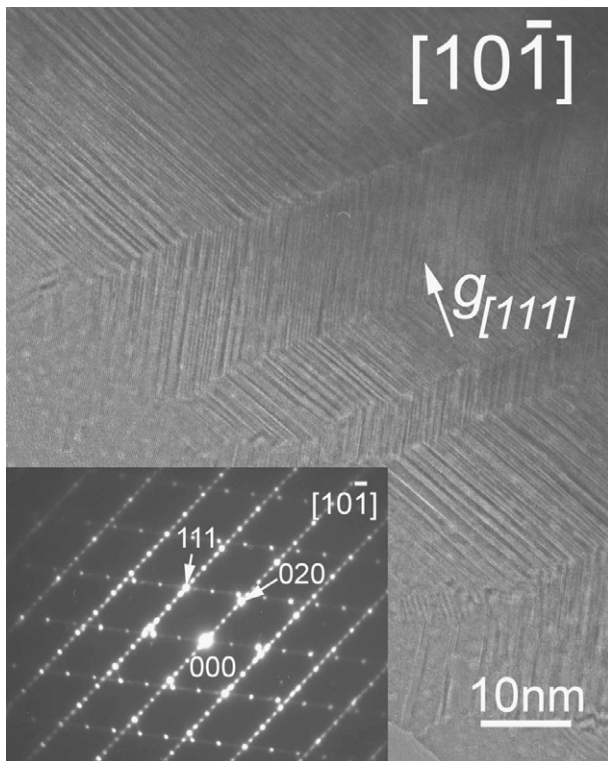


Fig. 4. Low-magnification HRTEM image and the corresponding diffraction pattern indexed assuming the expected B19 crystal structure showing twinning of the 33 long-period microtwin on $\{111\}_{B19}$ planes.

reveals macrotwinning on the same $\{111\}$ -type planes of the microtwinned plates (i.e. when retaining the B19 indexing). The martensite microstructure thus consists of areas showing only Type I macrotwinning and areas showing both Type I macrotwinning and compound microtwinning.

From such conventional bright and dark field TEM images the volume ratio λ of the small variant vs. the total width of two sequential twin variants for the B19 microtwinning can be calculated. For a thermoelastic martensitic transformation (here B2 to B19) with volume preservation this value is defined by the change in lattice parameters from austenite to martensite. A set of measurements is given in Table 1 together with the resulting average and standard deviation, $\lambda = 0.334 \pm 0.030$, which implies a variation of about 10%.

In Fig. 5 a $[1\bar{1}0]$ HRTEM image of a Type I macro-twin plane in the B19 structure is shown, revealing the atomic structure at the twin plane. The atomic resolution clearly shows a sharp and straight interface, but no evidence of microtwinning.

Fig. 6 shows two HRTEM images of the new long-period (LP) microtwin variant along the $[100]$ and $[101]$ zone axes, together with the corresponding SAED patterns. From the latter it can be concluded that the extra periodicity appears along the b -axis of the conventional B19 cell. In the central parts of these HRTEM images an $-ABCACB-$ stacking sequence along this axis can be recognized. In

Table 1

Volume ratio λ of microtwin variants as measured from eight different areas in Fig. 3 and yielding an average of 0.334 ± 0.030

λ_{meas}	0.27	0.265	0.46	0.25	0.44	0.33	0.38	0.28
-------------------------	------	-------	------	------	------	------	------	------

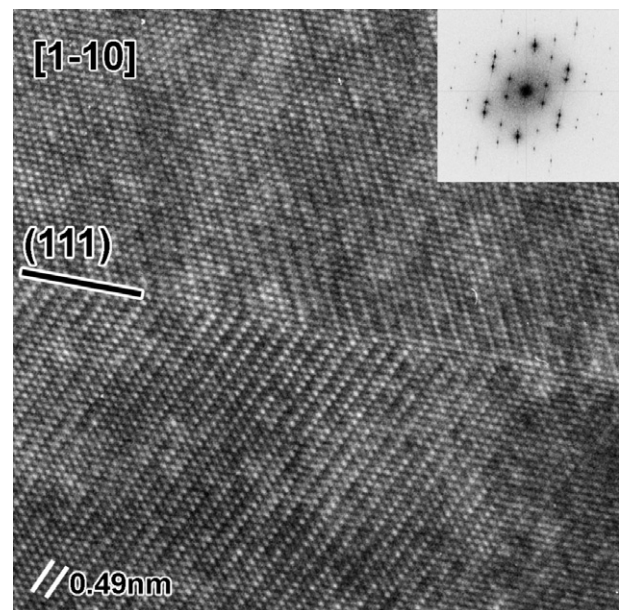


Fig. 5. Atomic resolution image of the Type I (111) twin interface. The inset is a power spectrum of the image, which also reveals the twinning.

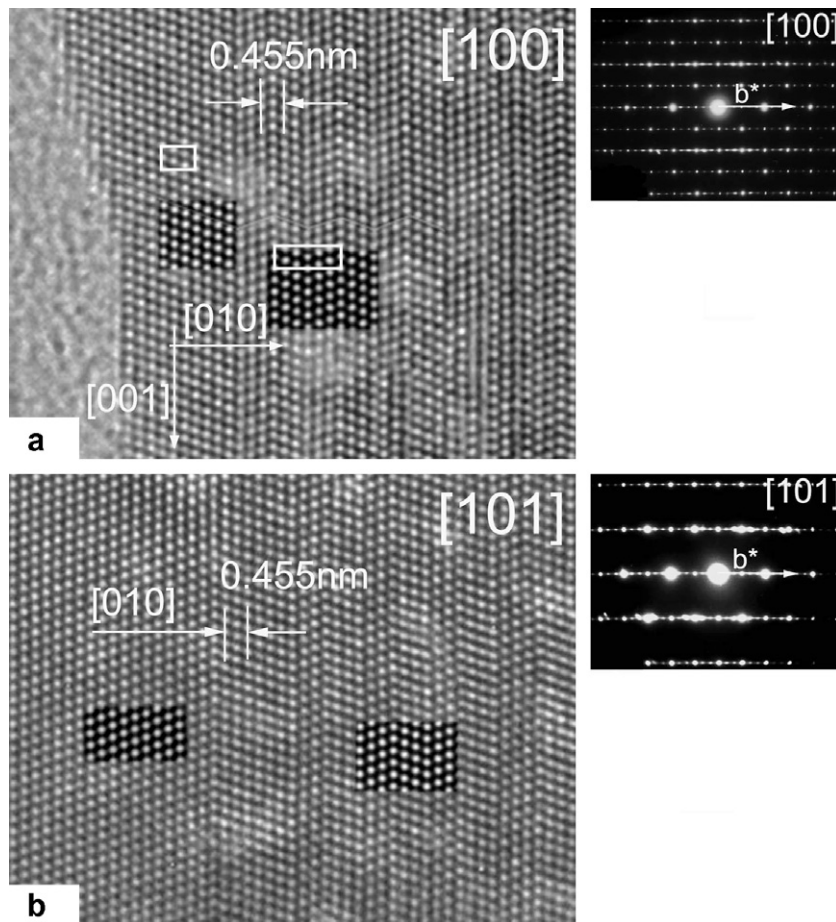


Fig. 6. Martensite HRTEM image revealing the ABC stacking as well as the $(3\bar{3})$ long-period microtwin variant with the incident beam parallel with the $[100]$ direction (a) and the $[101]$ direction (b), including the corresponding SAED patterns. The simulated HRTEM images and projected unit cell sizes are incorporated in (a) in order to confirm the proposed superstructure.

practice, however, the ideal stacking sequence is often violated, as seen on the right side of the HRTEM images, and results in streaking in the diffraction patterns along the $[010]_{B19^*}$ direction. Moreover, an $-ABC-$ type stacking in the same direction is observed close to the edge of the thinned area of the sample. Further to the right of these areas the sample rapidly becomes too thick for proper HRTEM.

EDX measurements, including the use of reference material to determine the k -factor, were performed in order to look for any difference in composition between the two apparent structures shown in Figs. 2 and 3. These measures confirm the intended equiatomic composition of the alloy, but no difference could be detected between plates with or without the long period within a precision of 2 at.%.

In order to evaluate the prevailing martensite structures in the alloy, X-ray powder diffraction and neutron powder diffraction measurements at $T = 20^\circ\text{C}$ were performed on a specimen in the shape of a cube ($a = 2$ mm). Neglecting the strong texture in the as-cast specimen, which strongly affects the peak intensities, the obtained diffraction patterns (Fig. 7a and b) could best be indexed using the orthorhombic B19 structure with lat-

tice parameters $a = 0.27615$ nm, $b = 0.45927$ nm and $c = 0.4838$ nm (± 0.00030 nm). The X-ray and neutron diffraction measurements yield the same lattice parameters, though the latter has a much larger error due to significant peak broadening. Neutron diffraction experiments were also carried out on the same sample after deformation in 7.7% compression and finally after heating to 1150°C for 10 min to recover the austenite phase followed by cooling back to martensite at room temperature (all using the same diffraction geometry). The results clearly indicate texture changes in the sample due to deformation in the martensite state. Moreover, preliminary in situ neutron diffraction experiments under loading and unloading indicate that the inelastic deformation is partially due to variant reorientation in the martensite, which implies a possible shape memory effect [11].

4. Discussion

For the orthorhombic B19 structure, only Type I twins with $K = \{111\}$ arranged in a quasi-periodic sequence of parallel twin planes were observed. According to the crystallographic theory of martensite (CTM) [12], such a

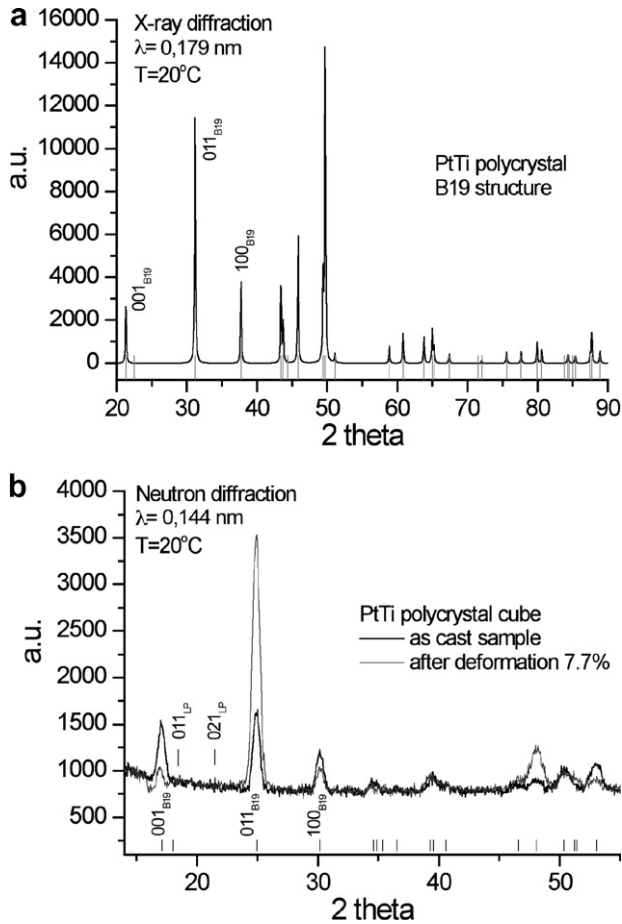


Fig. 7. X-ray (a) and neutron (b) powder diffraction spectra of PtTi martensite taken at room temperature. The neutron diffraction experiments were carried out on an as-cast cubic-shaped sample and on the same sample deformed 7.7% in compression (same geometry).

sequence of parallel Type I twins can indeed be formed in order to create a compatible austenite–martensite interface during transformation. The volume fraction λ of twin widths, defined as

$$\lambda = \text{width small variant} / \text{total width two subsequent variants}$$

then strongly depends on the lattice parameters of the austenite and martensite structures at the transformation temperature and can be calculated from [13]

$$\lambda = \frac{1}{2}(1 - \sqrt{1 + 2/\delta})$$

with

$$\delta = \mathbf{a} \cdot \mathbf{U}_I(\mathbf{U}_I^2 - \mathbf{I})^{-1} \mathbf{n}$$

where \mathbf{U}_I is the transformation matrix, \mathbf{I} is the unity matrix, \mathbf{a} is the vector of twinning shear and \mathbf{n} is the normal to the microtwin plane. For the present system, with $a_{B2} = 0.317$ nm [3] or 0.319 nm [1], the latter measured at 1100 °C, and room temperature B19 parameters as listed above, λ values between 0.12 and 0.22 are found as listed in Table 2. Comparing these values for the Type I case with

Table 2

Calculated value for the volume ratio λ based on the different combinations of presently measured (a , b , c B19) and literature (a_0 B2) lattice parameters

	a (nm)	b (nm)	c (nm)	a_0 (nm)	λ Type I
SAED	0.275	0.456	0.49	0.317 [3]	0.18
SAED	0.275	0.456	0.49	0.319 [1]	0.12
XRD	0.27615	0.45927	0.4838	0.317 [3]	0.22
XRD	0.27615	0.45927	0.4838	0.319 [1]	0.18

the experimentally measured ones, it can be concluded that the latter are on average substantially larger, i.e. the twin variants are more equal in width, but in some singular cases the ratio is substantially smaller (e.g. 0.25), although it never reaches the low theoretical values. The most obvious reason for this discrepancy is the lack of any lattice parameter data for the B19 structure at the transformation temperature where the microstructure is formed. When slightly larger values for the B19 lattice parameters are used in order to take lattice expansion at higher temperatures into account, the value for λ indeed increases. By following the rank-one connection condition in the CTM, it can further be shown that an interface between austenite and twinned martensite with Type II twins could also exist in the present system, but not with compound twins. However, no Type II twins were observed during the present study.

In order to determine the crystal structure and the space group of the LP structure several SAED tilting series were performed. In the primary analyses of these series only the strongest reflections from the diffraction patterns have been taken into account and a LP superstructure of the B19 basic structure has been considered. Starting from the expected crystal structure and the observation of the -ABC- or -ABCACB- stacking sequences along the b -axis, a structure model for the LP case appearing in the main part of the plates is proposed, as shown in Fig. 8a, together with the corresponding [100] projection revealing pure Ti or Pt columns. This structure has a $Pmm2$ space group and can be obtained considering a mechanism similar to that of Otsuka and Ren [2] for explaining the B2–B19 transformation and in which subsequent planes shuffle parallel with the basal $(110)_{B2}$ plane in both the $[1-10]$ and $[-110]_{B2}$ directions, as shown in Fig. 1. In Fig. 8b the same concept is used for constructing a structure model for the -ABC- stacking case observed at the extreme edge of the thinned sample. The corresponding projections for the B2 and B19 structures, i.e. along the $[001]_{B2}$ and $[100]_{B19}$ axes, are given in Fig. 8c and d, respectively, including an indication of the shuffles during the transformation for the latter.

To check the validity of these models, the resulting atomic parameters are used as input for simulations of SAED patterns as well as HRTEM images. The atomic positions are given in Table 3. Simulated SAED patterns for different structures along the $[100]_{B19}$ and $[101]_{B19}$ orientations are given in Fig. 9a–c and f–h.

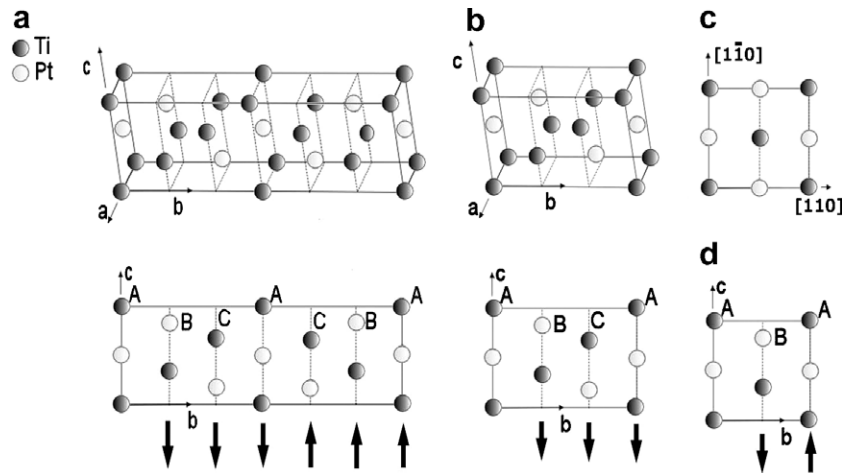


Fig. 8. (a) Proposed model for the orthorhombic unit cell of the $3\bar{3}$ long-period microtwin (perspective view and $[100]$ projection) with the lattice parameters $a_{LP} = a_{B19}$, $b_{LP} = 3b_{B19}$, $c_{LP} = c_{B19}$. (b) Proposed model for the orthorhombic unit cell with the $-ABC-$ stacking sequence (perspective view and $[100]$ projection) with the lattice parameters $a_{ABC} = a_{B19}$, $b_{ABC} = 1.5b_{B19}$, $c_{ABC} = c_{B19}$. (c) $[001]$ and (d) $[100]$ projections for B2 and B19 structures, respectively.

Table 3

The atomic positions of the $3\bar{3}$ long period unit cell and ABC unit cell with the x position at 0 for Ti and $1/2$ for Pt

No.	Type of unit cell					
	$3\bar{3}$ LP			ABC		
	y_{LP}	z_{Ti}	z_{Pt}	y_{ABC}	z_{Ti}	z_{Pt}
1	0	0	1/2	0	0	1/2
2	1/6	1/3	5/6	1/3	1/3	5/6
3	2/6	2/3	1/6	2/3	2/3	1/6
4	3/6	0	1/2			
5	4/6	2/3	1/6			
6	5/6	1/3	5/6			

As can be seen from Fig. 9a and f, some of the stronger reflections observed in the experimental SAED images, e.g. 022_{B19} (in the $[100]$ pattern) and 121_{B19} (in the $[101]$ pattern), cannot be explained just by assuming one of the new models as proposed in Fig. 8a and b, nor by taking multiple diffraction into account, a possibility which has been experimentally verified by tilting around the LP axis. On the other hand, these models are quite satisfactory for the HRTEM images (as can be seen from the inserted simulated high-resolution images in Fig. 6). The “missing” reflections from the simulation of the proposed structures can, however, be indexed in the B19 structure, which leads to the conclusion that this structure probably still exists in other, e.g. thicker, parts of the plate from where it enters the SAED pattern originating from an area of at least $0.5 \mu\text{m}$ diameter, i.e. much larger than the visible parts in the HRTEM images, due to the strong wedge shape of the edges of the thinned samples. In order to obtain consistent results from SAED patterns as well as from high-resolution images, the SAED patterns are considered as the result of four superimposed patterns: one corresponding to the $3\bar{3}$ long-period microstructure, two twin patterns

related by mirroring over the (010) plane and corresponding to the unit cell with $-ABC-$ stacking sequences, and one corresponding to the B19 structure. The separate patterns are given in Fig. 9a–c and f–h, with the summed patterns shown in Fig. 9d and i. The latter correspond much better with the observed SAED patterns originating from regions much larger than the HRTEM parts shown above.

As can be seen from the insets in Fig. 6, the HRTEM simulations fit very well with the observed white dot patterns, typical for ordered structures in this system [10,14]. It should be noted that the chosen conditions for these simulations assume a relatively low thickness of the sample (i.e. below 5 nm), which especially for the $[100]$ direction does not reveal the ordered nature of a binary column structure (i.e. white dots with different intensities) [10,14,15].

Although no clear preference in the TEM samples can be found for the B19 over the LP structure, the neutron and X-ray diffraction measurements only provide evidence for the B19 structure with no indication for the LP structure. Indeed, the LP structure would yield its first visible peaks (011) and (021) in between the 001 and 011 peaks of the B19 structure, an area showing no intensity above the noise in both scans. As the neutron diffraction originates from the bulk, this might suggest that the LP structure is a TEM sample preparation effect. In this view, the LP structure would be considered as induced by radiation impact from the ion-milling or by the thinning as such, i.e. as a thin film or surface relief effect. The fact that the HRTEM images reveal yet another stacking ($-ABC-$) on the extreme edges of the sample (around 3 nm in width) supports the possibility of the existence of such an effect. However, this could not be confirmed by cleaning the sample with aqua regia after the ion-milling, a procedure to remove surface radiation damage [10], since several LP areas were still observed, although this observation is hard

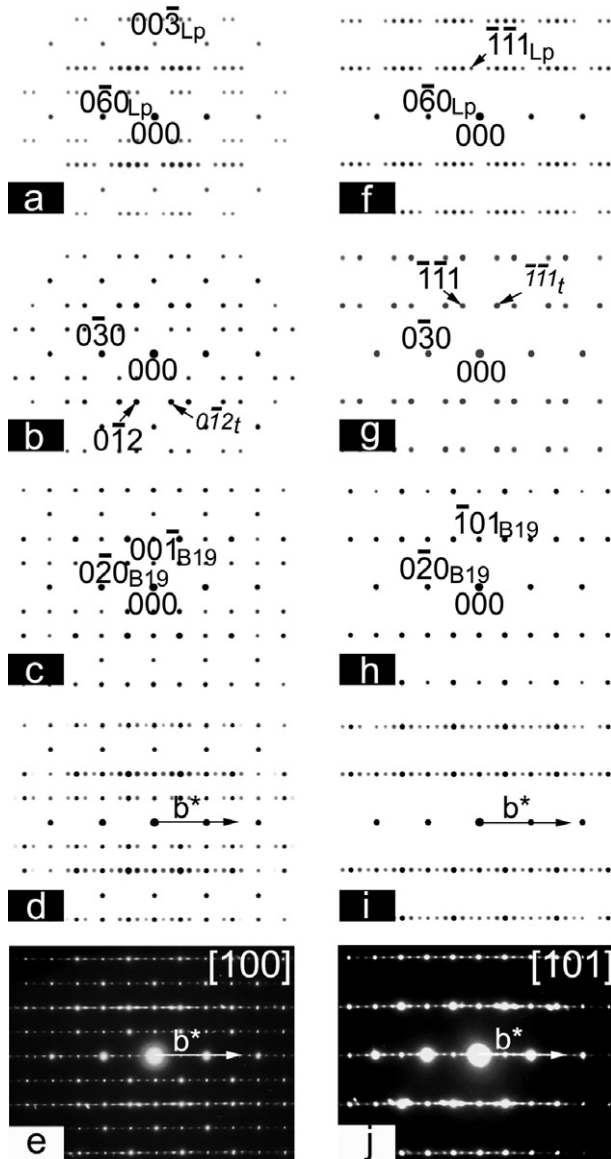


Fig. 9. Simulated diffraction patterns of the [100] (left column) and [101] (right column) zones of: the proposed long-period structure (a) and (f); two superimposed twins related by mirroring over (010) of the proposed structure with -ABC- stacking sequence (b) and (g); the B19 expected structure (c) and (h); and the resulting diffraction pattern after the superimposition of (a)–(c) for the [100] zone in (d), and (f)–(h) for the [101] zone in (i). Typical experimental SAED patterns of the [100] (e) and [101] (j) zones acquired from a region with -ABC- stacking and long-period microstructure as in Fig. 6.

to quantify. Moreover, thin edges revealing the -ABC- stacking have been observed previously in ion-milled Pt₃Ti material having the ordered -ABAC- stacking of the DO₂₄ structure [16], so the simple -ABC- stacking and not the more complex microtwin-like stackings appears to be a typical result from the ion-milling.

Also, the observation of two endothermic peaks upon heating in the dedicated DSC runs plus the data from the partial runs clearly linking the small endothermic peak upon heating with the shallow bump upon cooling both point to a possibly slightly inhomogeneous system in which

a small portion of the material transforms into a structure other than the expected B19 martensite. Whether or not this happens in a two-step fashion with the B19 as an intermediate is currently unclear, but the hysteresis of the small peaks and the large width of the shallow exothermic bump indicate a first-order transformation with possible influences from local stress inhomogeneities. The latter suggestion might explain why no difference in composition between the LP and B19 structures could be measured. Alternatively, when comparing the present DSC data of the large peaks with the values for the transformation temperatures for different compositions, as presented by Donkersloot Van Vucht [1], it is seen that in the present case the transformation temperatures are clearly below those for the perfect equiatomic composition, indicating a slight Pt enrichment of a few tens of atom percents. Moreover, the even lower values for the smaller peaks would indicate an even higher Pt content in the areas transforming at those values, albeit still within the precision of the EDX measurements, and possibly with a very small stability range.

Recently, similar LP structures have been found in ternary systems such as Ti₅₀Pt_xIr_(50-x) [17]. As the TEM samples of these materials were also ion-milled, these LP stackings could be induced by the ion-milling. On the other hand, the observation of a strong dependency of the periodicity on the composition indicates that these structures might be the proper low-energy structures for these alloys, with the actual stacking determined by the electronic structure of the alloy, as, for example, in Ni–Al- or Ni–Mn-based systems [18,19]. The latter argument plus the DSC observations and the possibility that the LP structure is formed after the B2–B19 transformation, thus leading to mixed areas of B19 and LP yielding the observed SAED patterns, leads us to conclude that also in the present binary system the LP structure is a low-energy structure, its existence possibly related to very small and local inhomogeneities in composition and/or stress. If this is the case, then the lack of any peaks corresponding to this LP structure in the X-ray and neutron diffraction data may be due to the fact that these were taken from a relatively large piece of material in which only a small portion of the LP structure would exist. Earlier X-ray work on Ti₅₀Pt_xIr_(50-x) alloys also did not recognize the LP structures later discovered by TEM [20].

5. Conclusions

A new martensite structure with a long-period stacking was found in equiatomic PtTi and the structure has been determined to be a $\underline{33}$ -type stacking by TEM. The presence of Type I {111} twins in the B19 and LP structures are reported. The observed electron diffraction patterns revealing the LP structure can best be explained as a mixture of four structures (one $\underline{33}$ long-period microstructure, two-twin related regions with the -ABC- stacking sequences and the expected B19 structure). Although X-ray and neutron powder diffraction from bulk material could not

reveal the new long-period structure, multiple peaks in a DSC run and a comparison with similar systems indicate that this new LP structure is not due to radiation damage from the ion-milling but might be due to slight composition or stress inhomogeneities leading to mixed B19 and LP regions.

Acknowledgements

This article was written in honour of Severin Amelinckx. G.-M. Rotaru thank MULTIMAT “Multi-scale modeling and characterisation for phase transformations in advanced materials”, a Marie Curie Research Training Network (MRTN-CT-2004-505226) and the University of Antwerp for supporting this work. Part of this work was also performed in the framework of an FWO research project G.0465.05 “The functional properties of shape memory alloys: a fundamental approach”.

References

- [1] Donkersloot HC, Van Vucht JHN. *J Less-Common Met* 1970;20:83–91.
- [2] Otsuka K, Ren XB. *Intermetallics* 1999;7:511–28.
- [3] Ye YY, Chan CT, Ho KM. *Phys Rev B* 1997;56:3678–89.
- [4] Huang X, Rabe KM, Ackland GJ. *Phys Rev B* 2003;67:024101–8.
- [5] Dwight AE, Conner Jr RA, Downey JW. *Acta Crystallogr* 1965;18:835–9.
- [6] Biggs T, Witcomb MJ, Cornish LA. *Mater Sci Eng A* 1999;273–275:204–7.
- [7] Biggs T, Cortie MB, Witcomb MJ, Cornish LA. *Metall Mater Trans A* 2001;32:1881–6.
- [8] Biggs T, Cortie MB, Witcomb MJ, Cornish LA. *Platinum Met Rev* 2003;47:142–56.
- [9] Noolu NJ, Kerr HW, Zhou Y, Xie J. *Mater Sci Eng A* 2005;397:8–15.
- [10] Schryvers D, Amelinckx S. *Acta Metall* 1986;34:1245–55.
- [11] Lukas P. Nuclear Physics Institute v.v.i Academy of Sciences of the Czech Republic, Rez near Prague, Czech Republic, personal communication.
- [12] Ball JM, James RD. *Arch Ration Mech Anal* 1987;100:13; Ball JM, James RD. *Philos Trans R Soc Lond A* 1992;338:389.
- [13] Bhattacharya K. *Microstructure of martensite*. Oxford: Oxford University Press; 2003, ISBN 0-19-8509340. p. 113.
- [14] Schryvers D, Amelinckx S. *Res Mech* 1987;22:101–49.
- [15] Van Dyck D. *Adv Imag Electr Phys* 2002;123:105–71.
- [16] Schryvers D. “Order–disorder phenomena in the binary alloys Pt_xTi, Pt_xV (3 ≤ x ≤ 8) and Ni₃Mo studied by HREM”, PhD thesis, University of Antwerp, 1985.
- [17] Hara T, Yamabe-Mitarai Y, Okunishi E, Sawada H. In: Ichinose H, Sasaki T, editors. *Proceedings of IMC16, Sapporo*, vol. III, 2006. p. 1649–50.
- [18] Schryvers D, Tanner LE. *Trans MRS Jpn* 1994;18B:849–52.
- [19] Morito S, Kakeshita T, Hirata K, Otsuka K. *Acta Mater* 1998;46:5377–84.
- [20] Yamabe-Mitarai Y, Hara T, Hosoda H. *Mater Sci Forum* 2003;426–432:2267–72. *Proc THERMEC* 2003.